SUPPORTING INFORMATION

of

Structural Characterization, Proton Conductivity and Furfural Catalysis of Novel Polyfunctional Zirconium Phosphonates

Montse Bazaga-García,[a,b] *Rosario M. P. Colodrero,* [a,c] *Álvaro Vílchez-Cózar,* [a,c] *Pascual Olivera-Pastor,* [a,c] *Juan A. Cecilia,* [a,d] *Łukasz Kurowski,* [e] *Jan K. Zaręba,* [*,e] *Aurelio Cabeza* [a,c,*]

[a] Departamento de Química Inorgánica, Cristalografía y Mineralogía, Facultad de Ciencias, Universidad de Málaga, Campus Teatinos s/n 29071-Málaga, Spain

[b] Departamento de Química Inorgánica, Universidad de Salamanca, Plaza de los Caídos s/n, 37008 Salamanca, Spain.

[c] Instituto Universitario de Materiales y Nanotecnología, IMANA, Universidad de Málaga, Campus Teatinos s/n 29071-Málaga, Spain

[d] Instituto de Investigación de Biorrefinerías "I3B", Facultad de Ciencias, Universidad de Málaga, Campus Teatinos s/n 29071-Málaga, Spain

[e] Department of Chemistry, Wrocław University of Technology, 27 Wybrzeze Wyspianskiego Str., 50-370 Wrocław, Poland.

Table of contents

Figures

Tables

Table S1. Rietveld analysis for **Zr-BTTMP** at different conditions under N_2 from thermodiffraction ($Cu_{K\alpha 1}$) data.

Table S2. Conversion and product yields for FUR transformation on Zr-based catalysts.

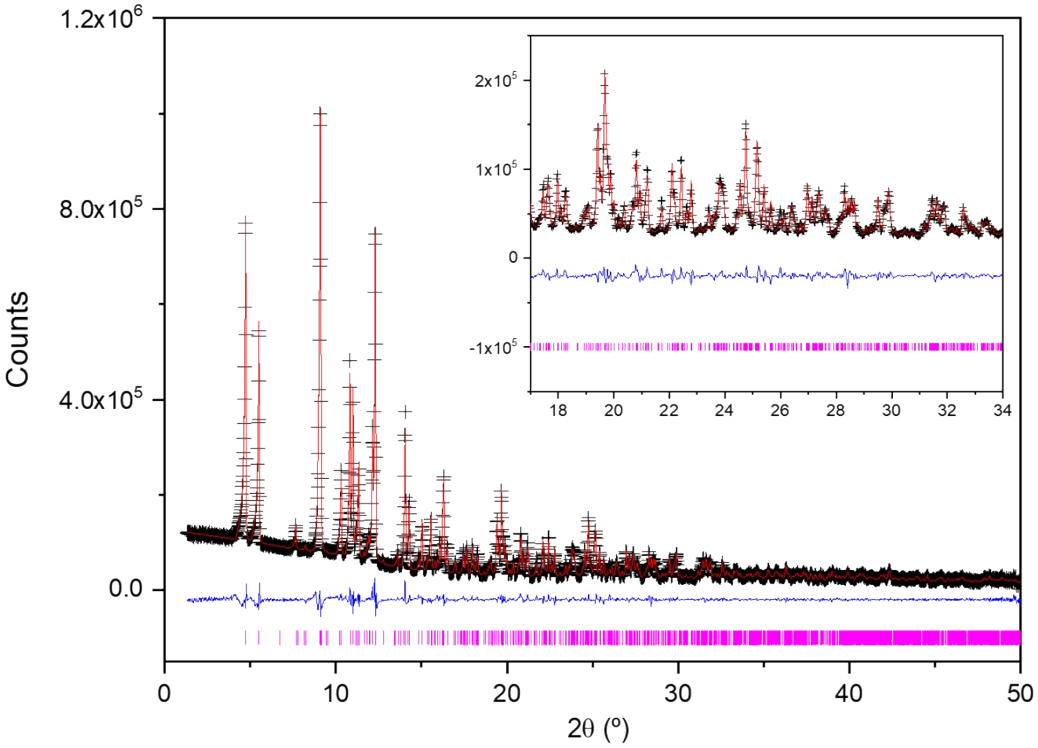

Figure S1. Rietveld plot for $Zr(O_3P\text{-}NH\text{-}C_5H_3\text{-}COOH)_2F_2$ **(Zr-PNA)**.

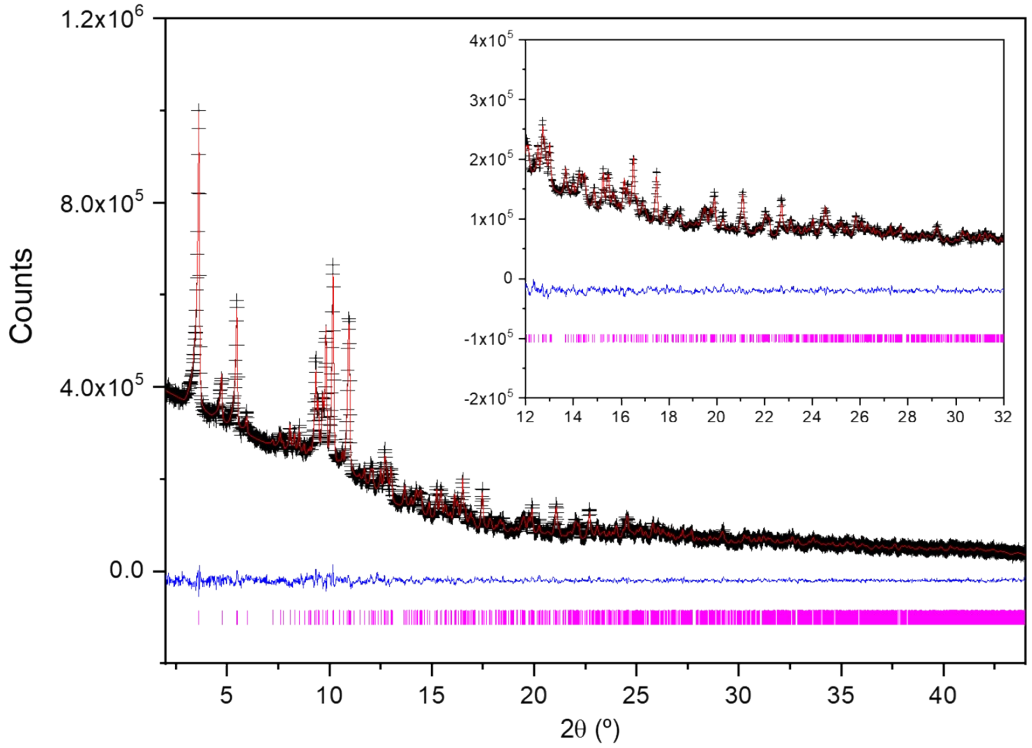

Figure S2. Rietveld plot for $Zr[(H_2O_3PCH_2)(O_3PCH_2)_2\text{-}C_6H_3]\cdot H_2O$ **(Zr-BTTMP)**.

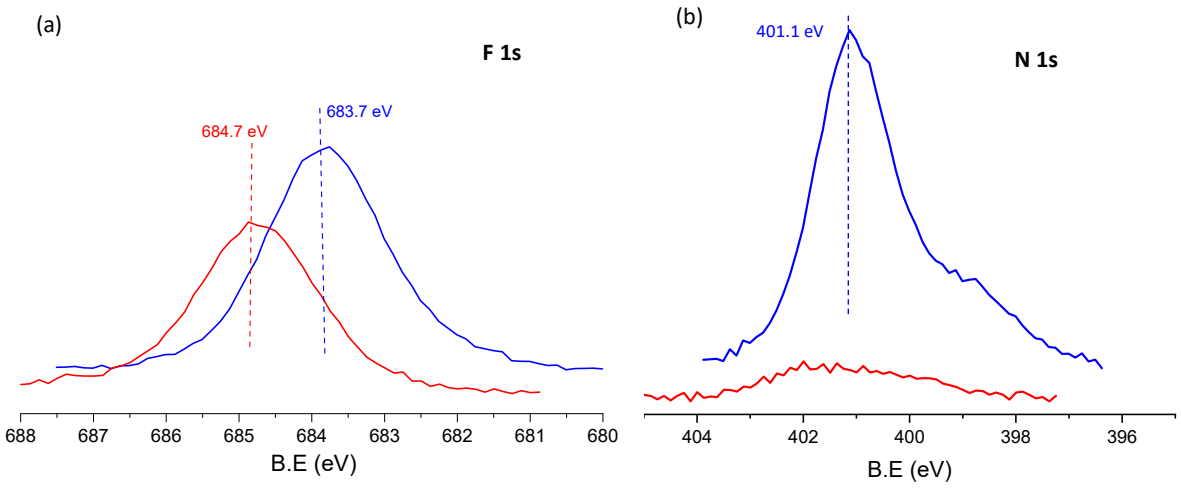

Figure S3. XPS spectra of (a) F 1s and (b) N 1s for **Zr-PiPhtA** (red) and **Zr-PNA** (blue).

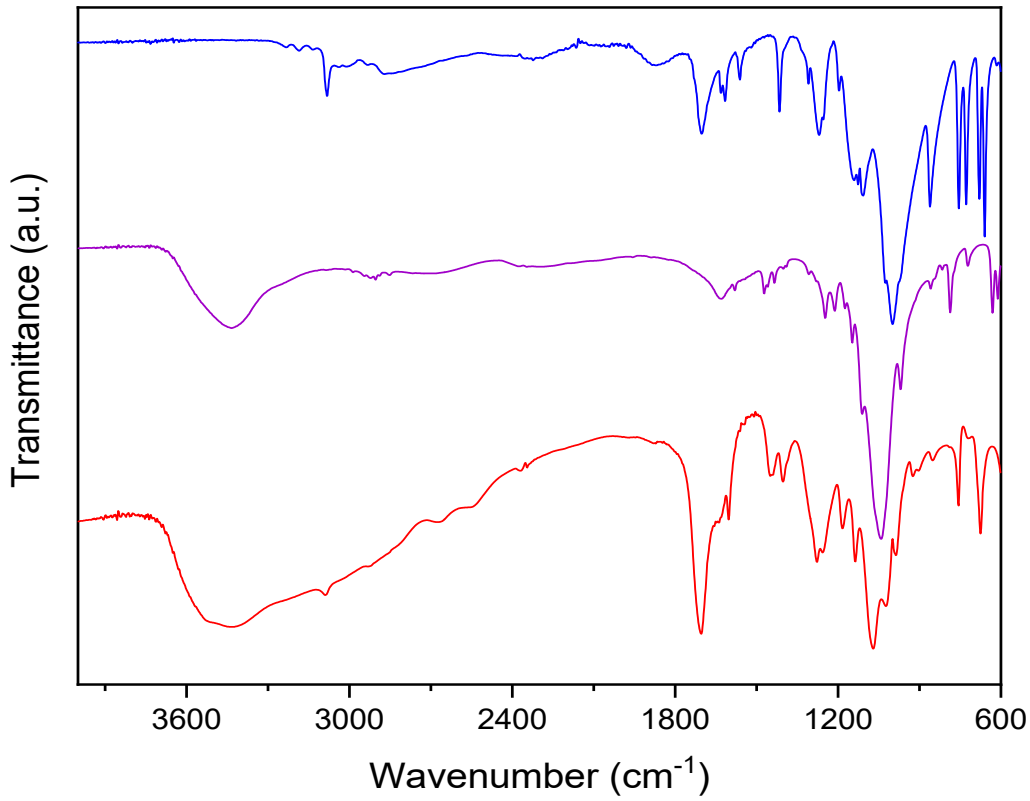

Figure S4. FT-IR spectra for **Zr-PNA** (blue), **Zr-BTTMP** (violet) and **Zr-PiPhtA** (red).

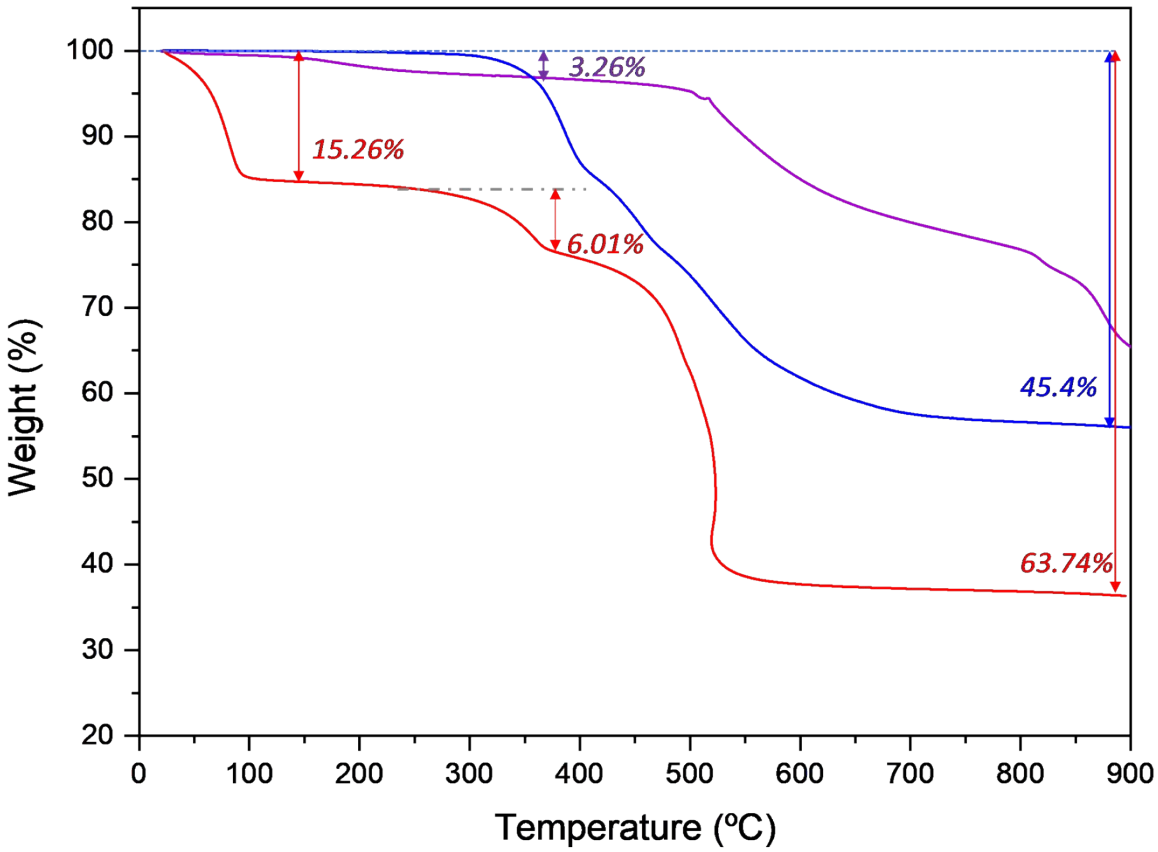

Figure S5. Thermal analysis for **Zr-PNA** (blue), **Zr-BTTMP** (violet) and **Zr-PiPhtA** (red).

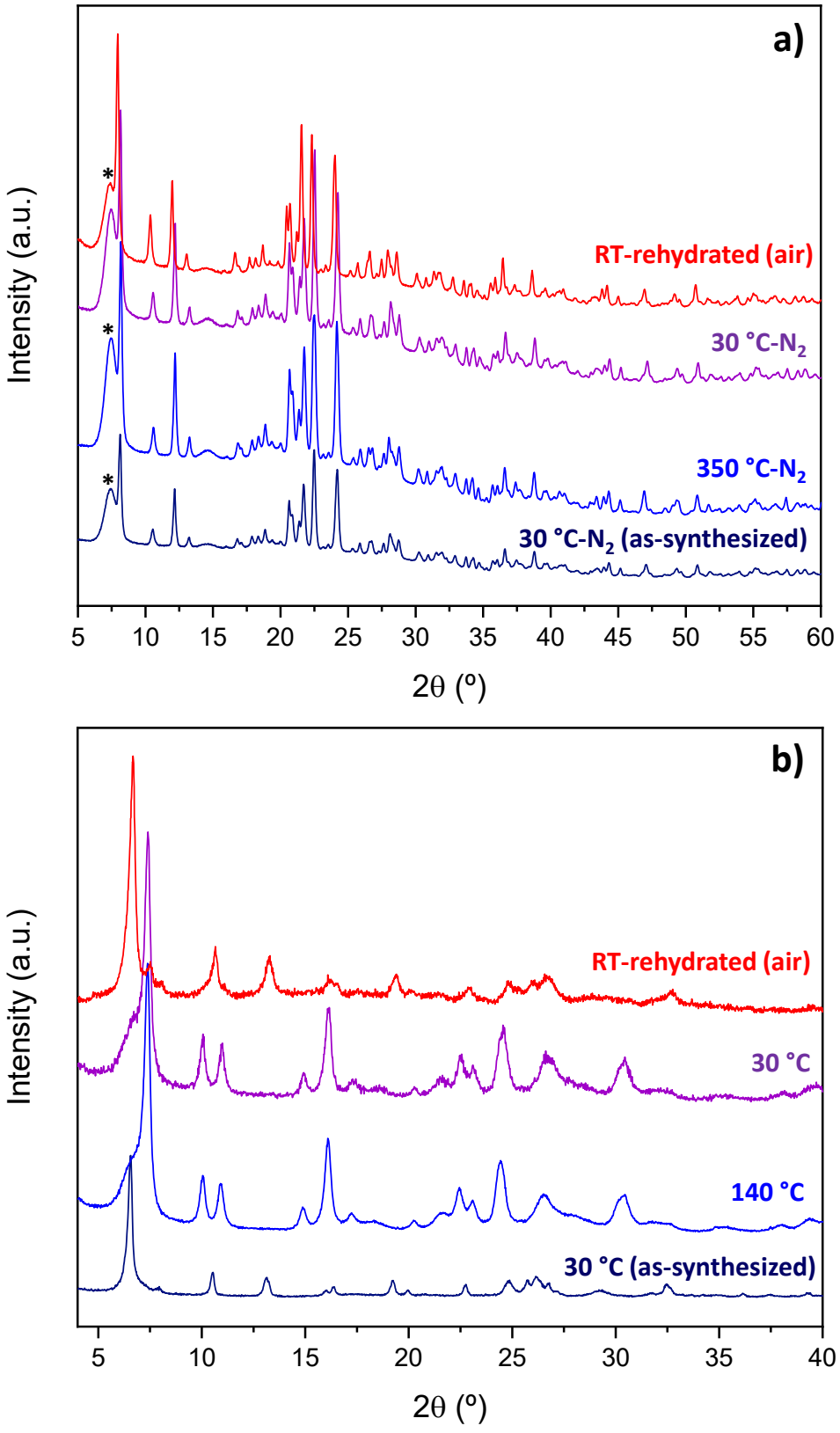

Figure S6. X-ray thermodiffraction patterns of (a) **Zr-BTTMP** and (b) **Zr-PiPhtA**. (*peak corresponding to the chamber).

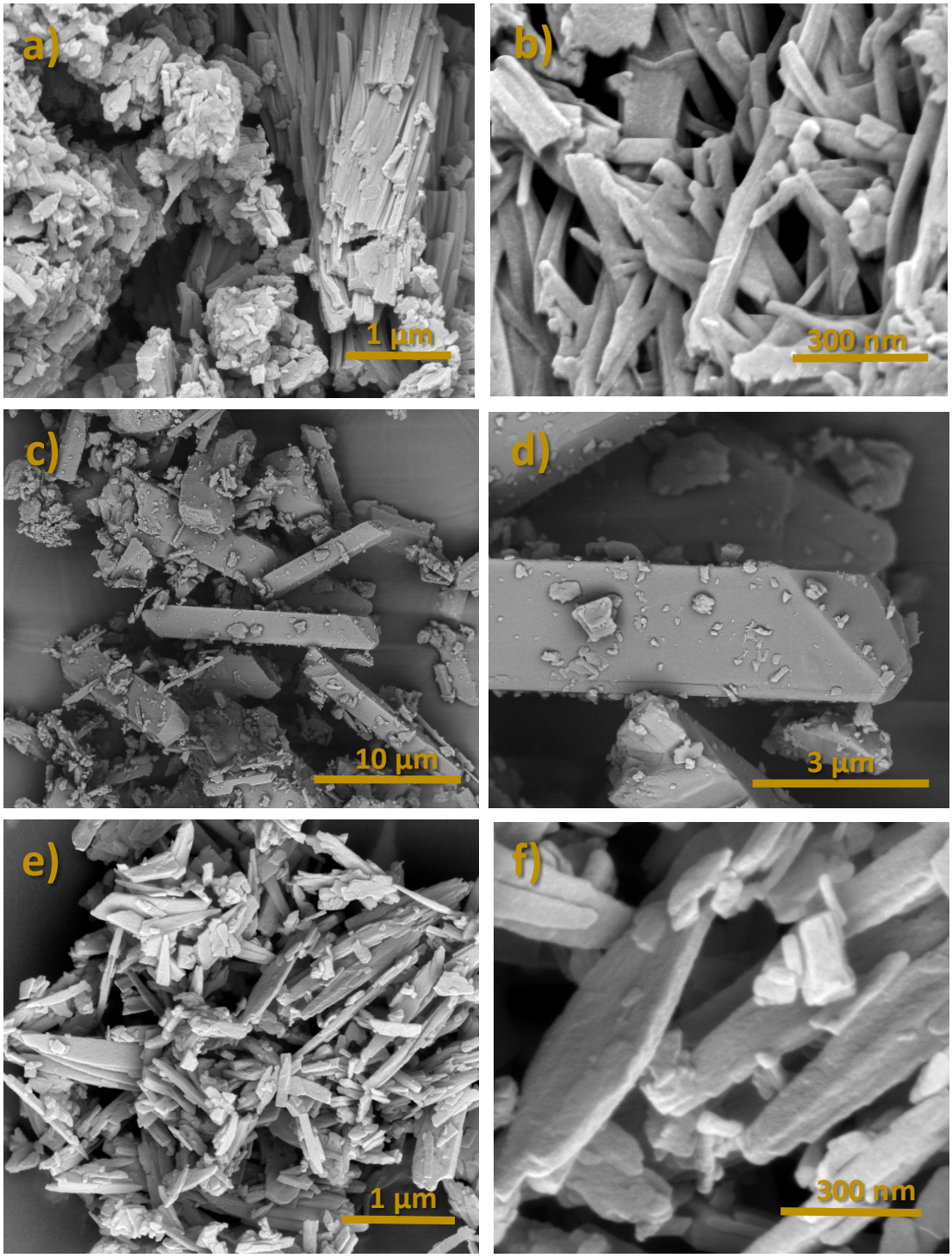

Figure S7. SEM images for (a, b) **Zr-PiPhtA**, (c, d) **Zr-PNA** and (e, f) **Zr-BTTMP**.

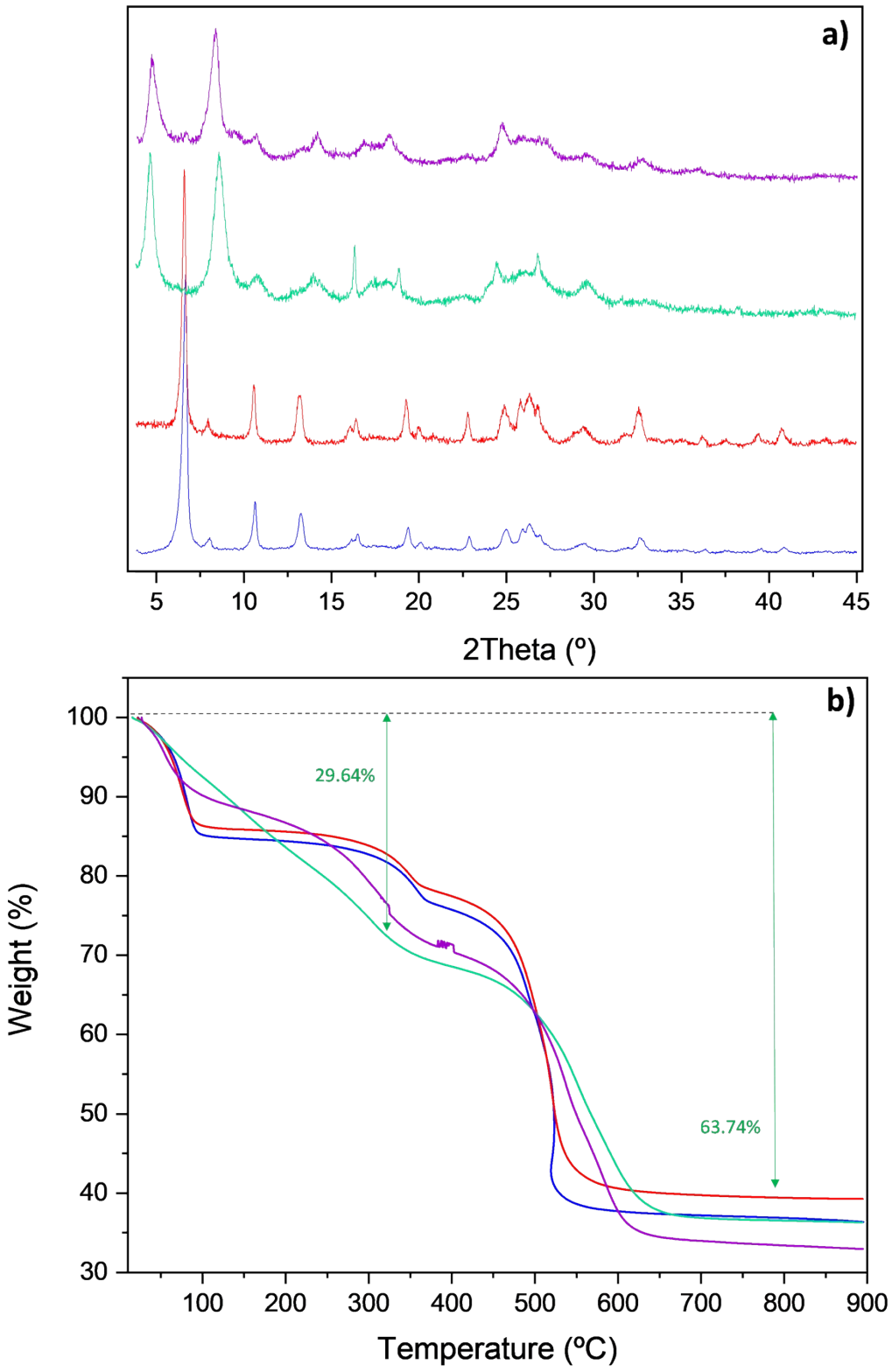

Figure S8. (a) X-ray powder diffraction (XRPD) patterns and (b) TG analysis for **Zr-PiPhtA** (blue), **Zr-PiPhtA_NH$_3$** (green), and post-impedance **Zr-PiPhtA** (red) and **Zr-PiPhtA_NH$_3$** (violet) samples.

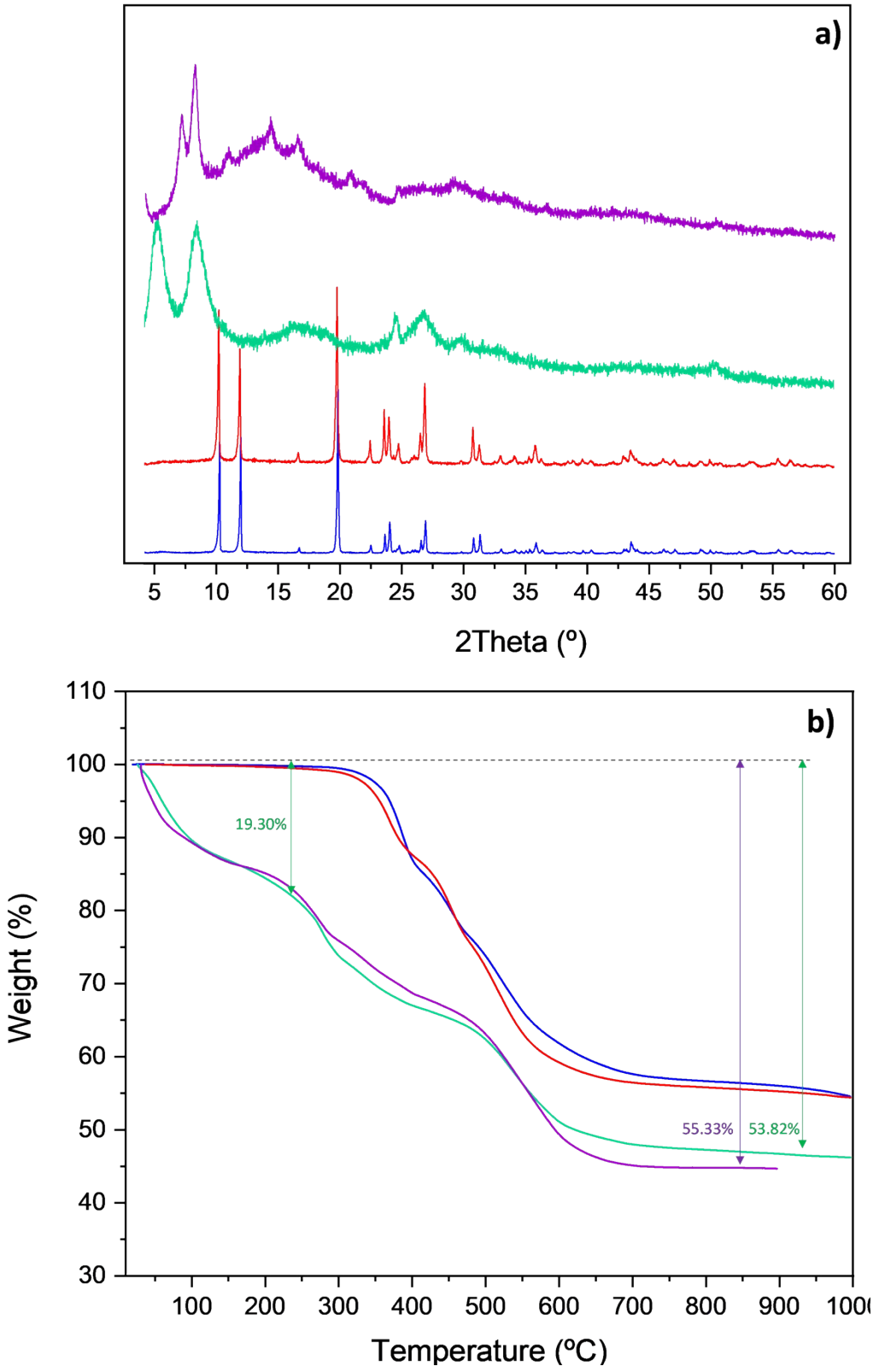

Figure S9. (a) X-ray powder diffraction (XRPD) patterns and (b) TG analysis for **Zr-PNA** (blue), **Zr-PNA_NH$_3$** (green), and post-impedance **Zr-PNA** (red) and **Zr-PNA_NH$_3$** (violet) samples.

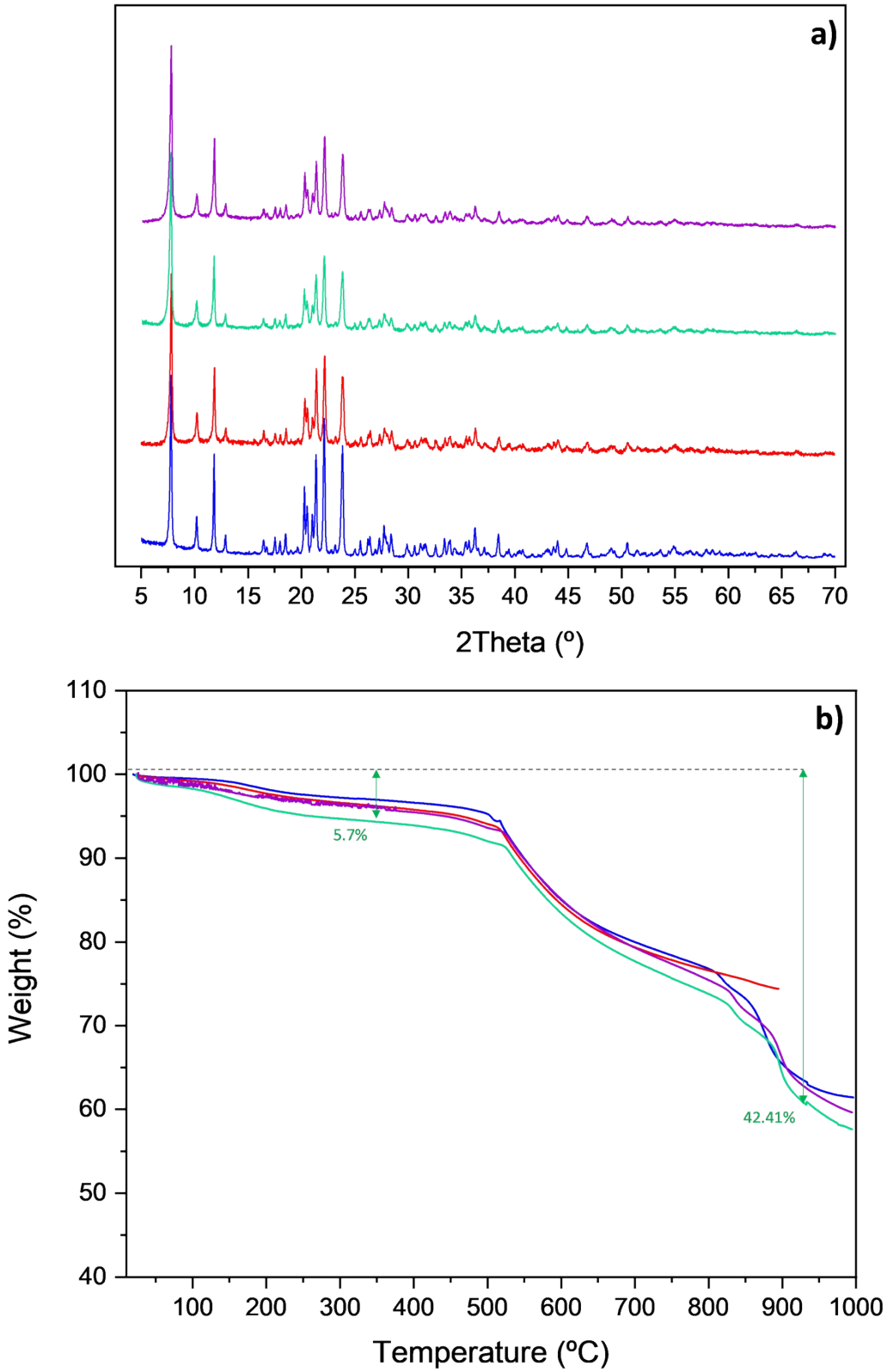

Figure S10. (a) X-ray powder diffraction (XRPD) patterns and (b) TG analysis for: **Zr-BTTMP** before (blue), **Zr-BTTMP_NH$_3$** (green), and post-impedance **Zr-BTTMP** (red) and **Zr- BTTMP_NH$_3$** (violet) samples.

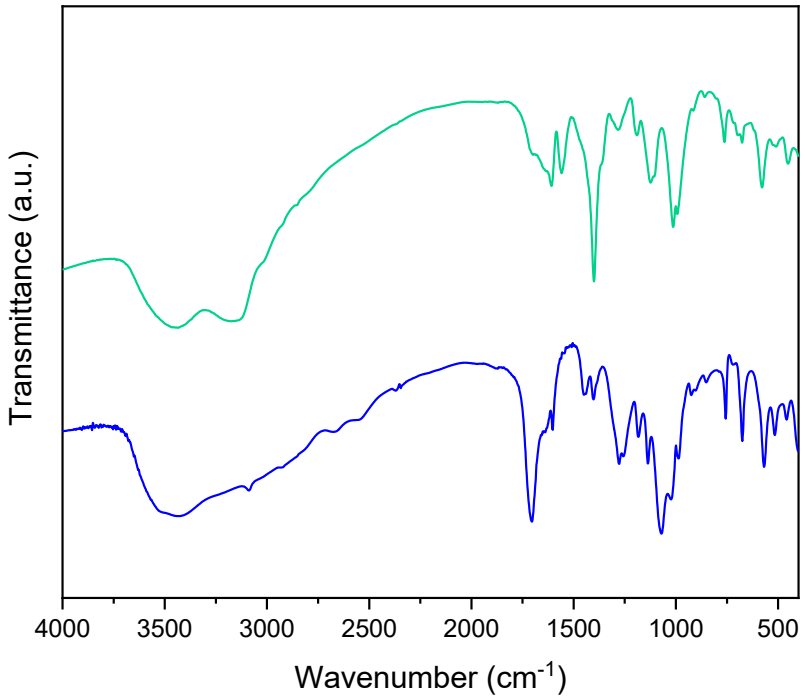

Figure S11. FT-IR spectra of **Zr-PiPhtA** as synthetized (blue) and **Zr-PiPhtA_NH$_3$** (green).

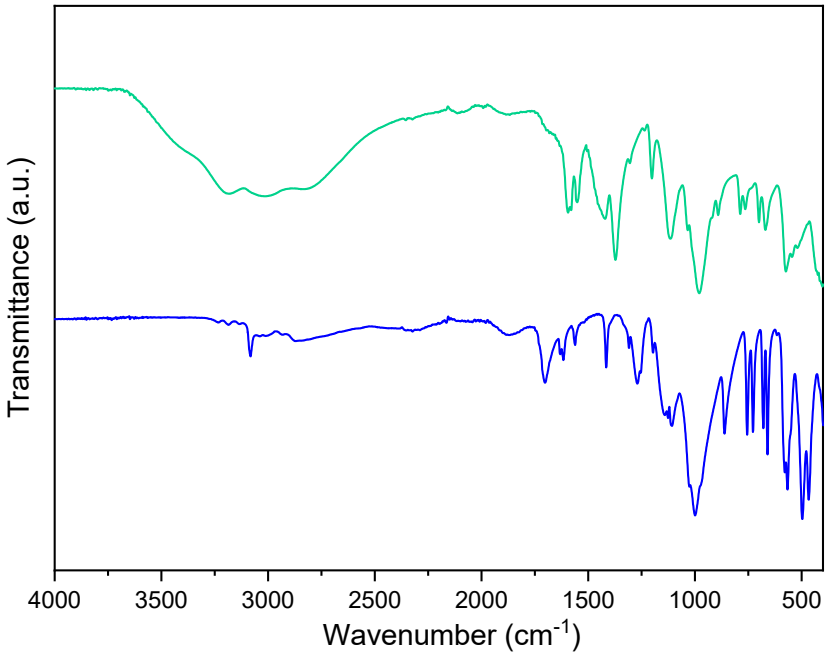

Figure S12. FT-IR spectra for **Zr-PNA** as synthetized (blue) and **Zr-PNA_NH$_3$** (green).

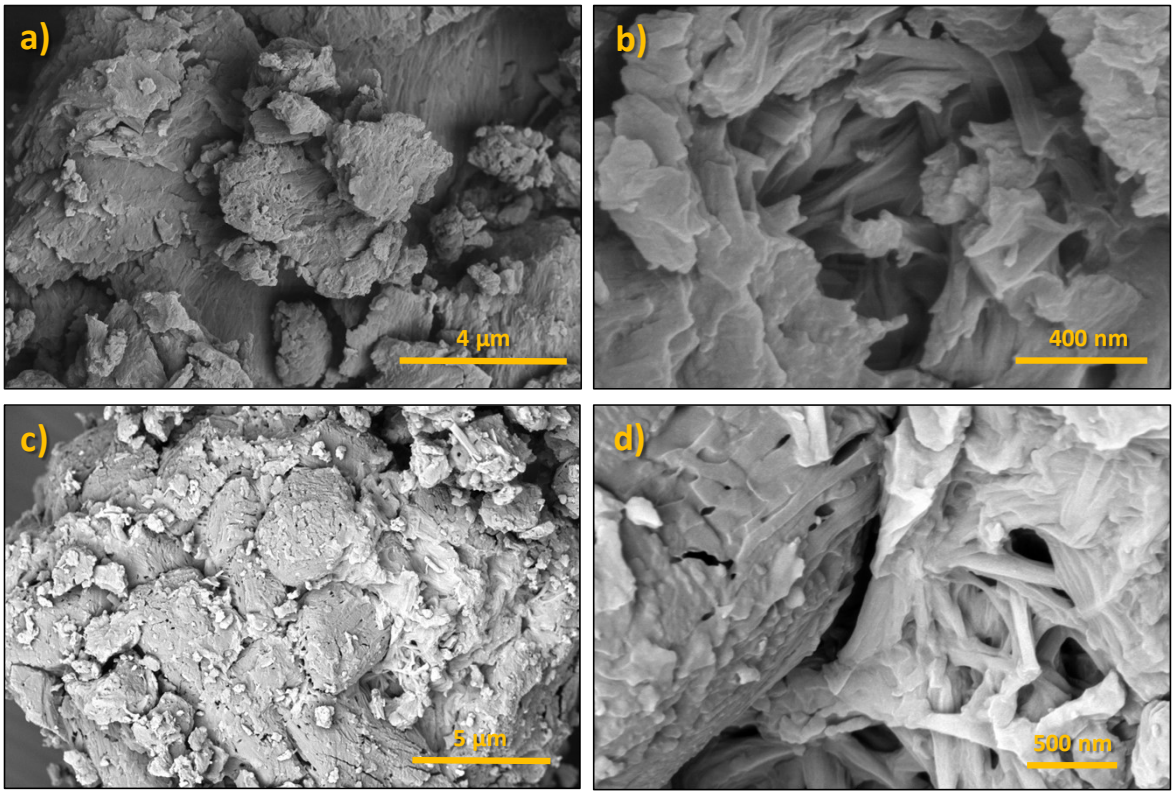

Figure S13. SEM images for (a, b) **Zr-PiPhtA_NH$_3$** and (c, d) **Zr-PNA_NH$_3$**.

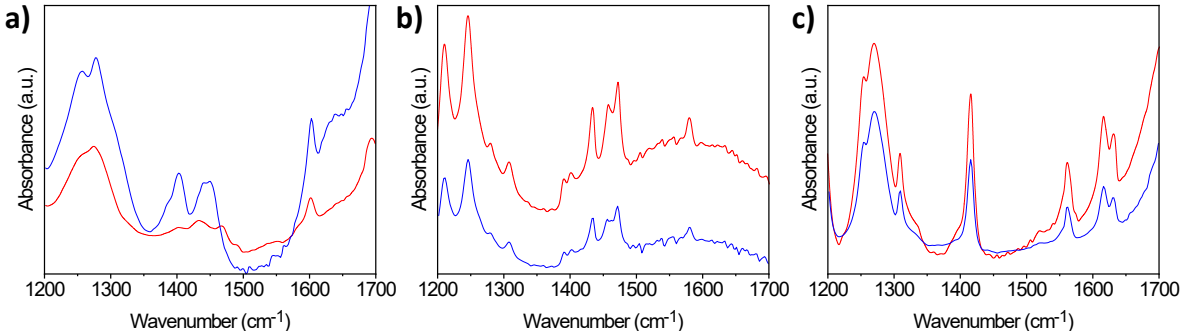

Figure S14. FT-IR spectra for (a) **Zr-PiPhtA**, (b) **Zr-BTTMP** and (c) **Zr-PNA** as synthetized (red) and pyridine-adsorbed samples (blue).

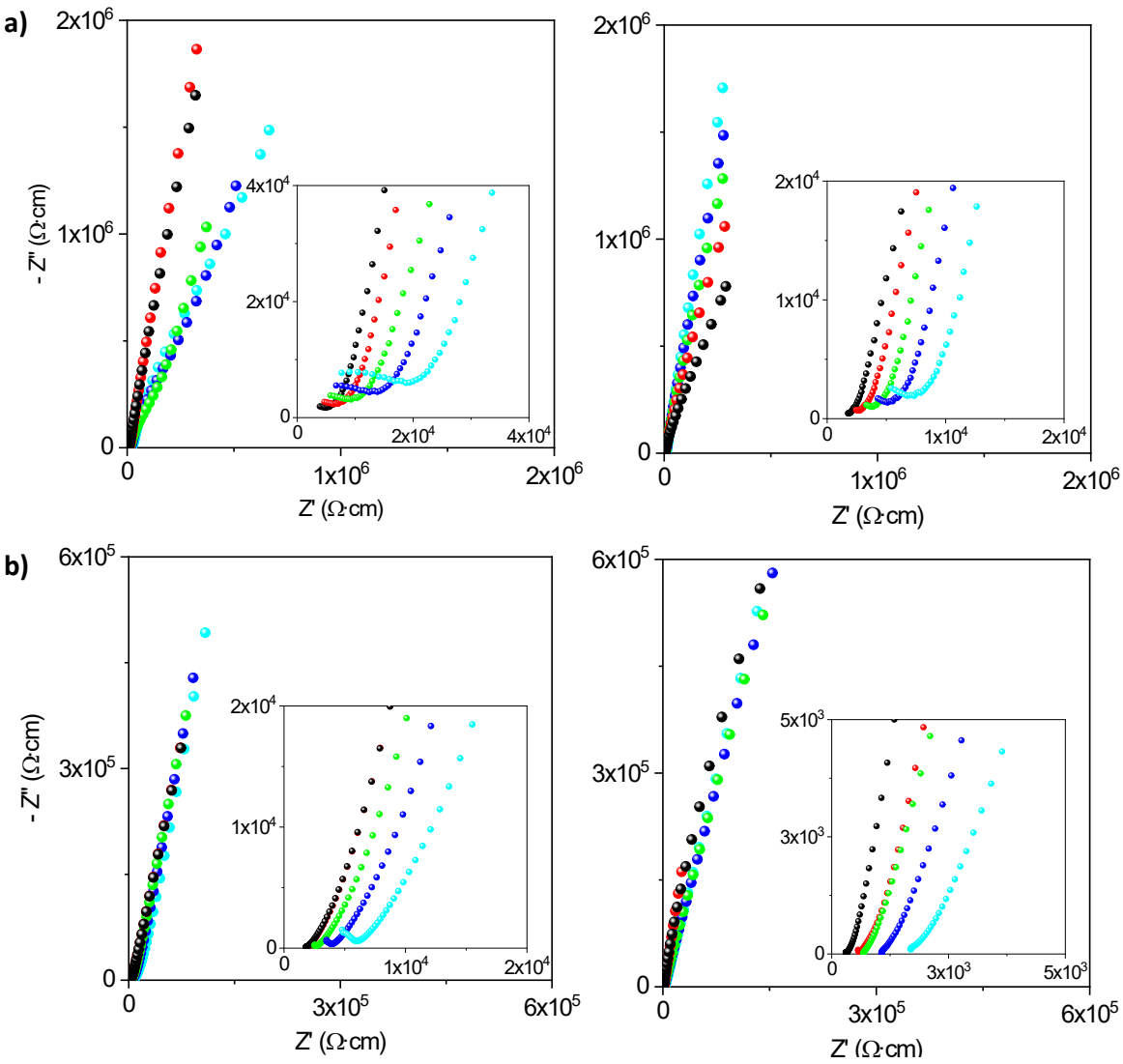

Figure S15. Plot of complex impedance plane for (a) **Zr-PiPhtA** and (b) **Zr-PiPhtA_NH$_3$** compound at 75% (left) and 95% (right) of relative humidity (RH) at different temperatures: 80 (black), 70 (red), 60 (green), 50 (blue) and 40 ºC (cyan).

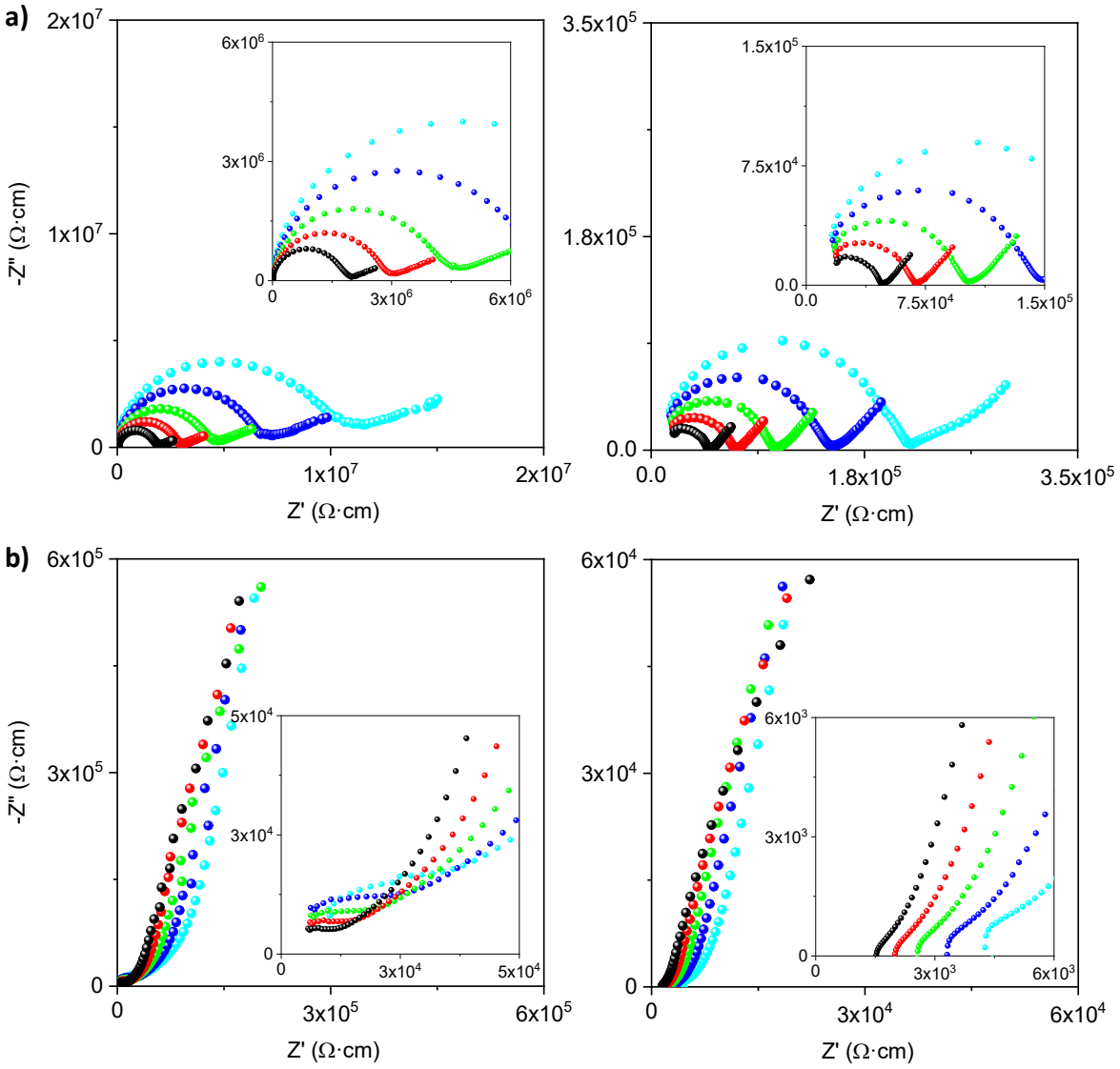

Figure S16. Plot of complex impedance plane for (a) **Zr-PNA** and (b) **Zr-PNA_NH$_3$** compound at 75% (left) and 95% (right) of relative humidity (RH) at different temperatures: 80 (black), 70 (red), 60 (green), 50 (blue) and 40 ºC (cyan).

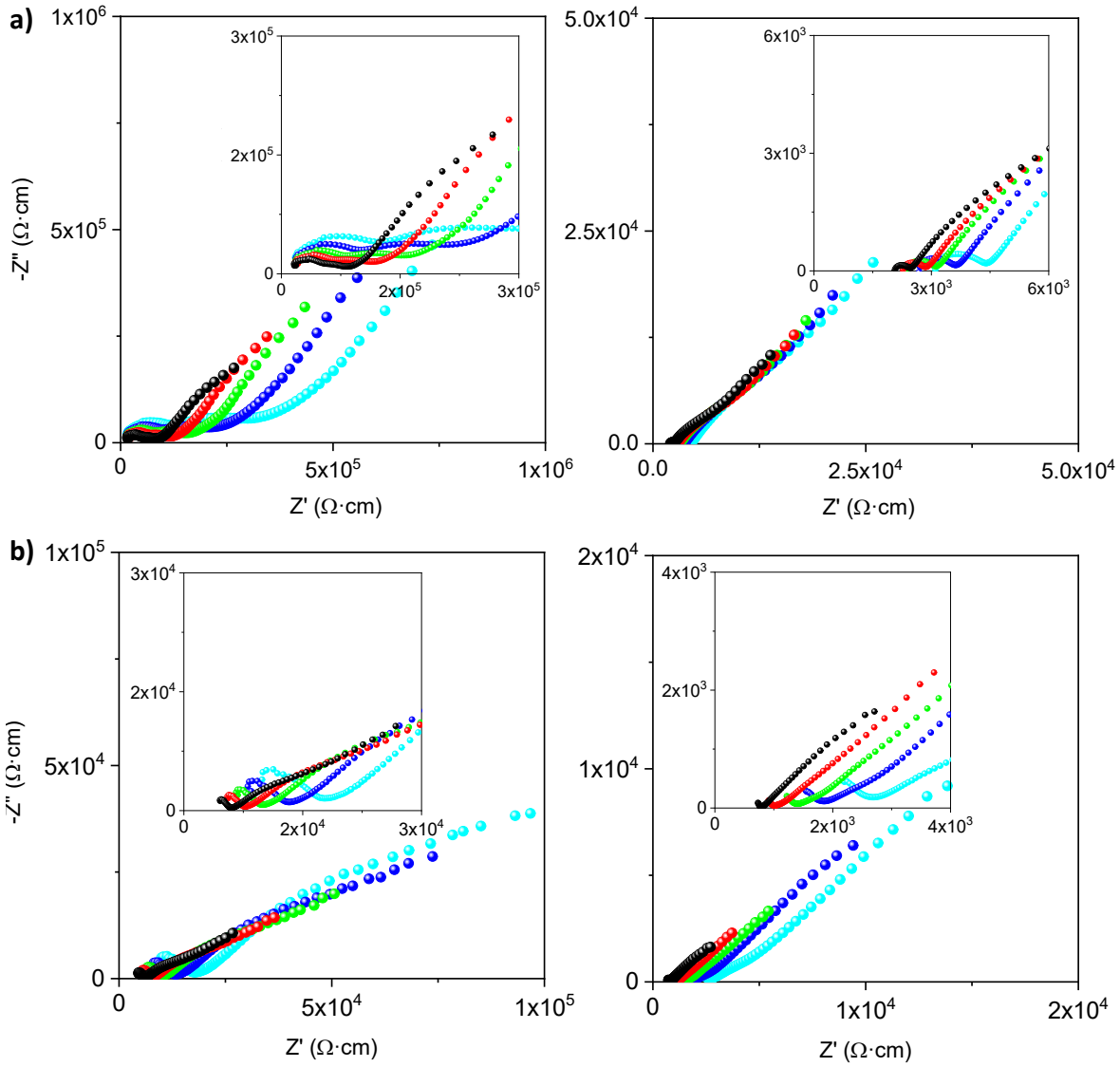

Figure S17. Plot of complex impedance plane for (a) **Zr-BTTMP** and (b) **Zr-BTTMP_NH$_3$** at 75% (left) and 95% (right) of relative humidity (RH) at different temperatures: 80 (black), 70 (red), 60 (green), 50 (blue) and 40 ºC (cyan).

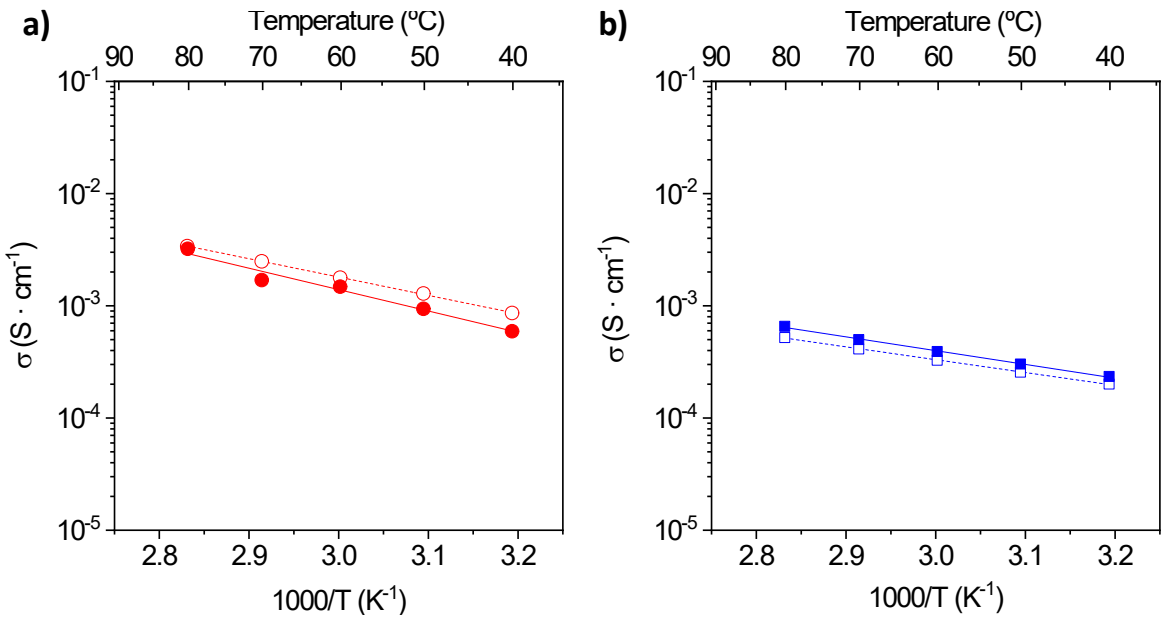

Figure S18. Arrhenius plots at 95% RH of first (closed symbols) and second (open symbols) cycle samples: (a) **Zr-PiPhtA_NH$_3$** and (b) **Zr-PNA_NH$_3$**.

Table S1. Rietveld analysis for **Zr-BTTMP** at different conditions under N_2 from thermodiffraction ($Cu_{K\alpha1}$) data.

Compound	**As-synthesized**	**350 ºC-N_2**	**30 ºC-N_2**
***a* (Å)**	15.0070(30)	15.0451(28)	14.9954(30)
***b* (Å)**	17.2903(21)	17.3074(20)	17.2805(21)
***c* (Å)**	5.3002(8)	5.3164(7)	5.2968(8)
***β* (°)**	95.483(7)	95.293(6)	95.547(7)
Volume (Å^3)	1369.0(4)	1378.4(4)	1366.1(4)
Z	4	4	4
ρ_{calc} (g·cm^{-3})	2.1166	2.1060	2.1210
2θ range (°)	7.3–67.1	7.3–67.1	7.3–67.1
Data/restraints/parameters	2991/525/99	3582/526/99	2986/525/99
R_{wp}	7.05	6.53	6.40
R_p	5.32	4.85	4.82
R_F	5.67	5.43	5.44

Table S2. Conversion and product yields for FUR transformation on Zr-based catalysts

Catalyst	Reaction time (h)	FUR conversion (%)	Yields (%)			
			FOL	IpFE	IpL	ND*
Zr-PNA	0	0	0	0	0	0
	3	6.5	3.7	2.3	0	0.4
	6	19.2	5.4	3.1	0.4	10.3
	9	24.1	6.7	4.0	1.2	12.2
	12	28.0	7.4	6.9	2.6	11.1
	24	37.1	7.6	13.9	4.5	11.1
Zr-PiPhtA	0	0	0	0	0	0
	3	28.6	9.1	14.9	1.8	2.8
	6	40.5	14.1	18.2	3.7	4.4
	9	54.2	19.0	21.7	4.4	9.1
	12	63.4	19.7	29.1	7.4	7.3
	24	81.2	18.9	37.6	12.4	13.1
Zr-BTTMP	0	0	0	0	0	0
	3	40.4	13.7	19.0	3.6	4.1
	6	49.4	15.6	22.1	5.5	6.2
	9	64.3	23.3	23.4	5.4	12.2
	12	81.9	19.6	34.6	9.6	18.1
	24	100	17.2	44.4	16.6	21.8
$Zr_3(PO_4)_4$	0	0	0	0	0	0
	3	17.2	11.5	0	0	5.7
	6	32.3	24.8	0	0	7.5
	9	38.5	21.4	3.9	1.4	11.8
	12	46.7	19.0	7.2	8.3	16.3
	24	63.0	18.8	12.9	12.3	19.0

*ND: non-detected products